A comprehensive investigation of the interactions of human serum albumin with polymeric and hybrid nanoparticles

Merve Seray Ural, Joice Maria Joseph, Frank Wien, Xue Li, My-An Tran, Myriam Taverna, Ruxandra Gref, Claire Smadja

A comprehensive investigation of the interactions of human serum albumin with polymeric and hybrid nanoparticles

Merve Seray Ural [a,b], Joice Maria Joseph [a,b], Frank Wien [c], Xue Li [a], My-An Tran [a], Myriam Taverna [b], Claire Smadja [b*], Ruxandra Gref [a*]

[a] Université Paris-Saclay, Institute of Molecular Sciences of Orsay, French National Center for Scientific Research, Orsay, France
[b] Université Paris-Saclay, Institut Galien Paris-Saclay, UMR CNRS 8612, French National Center for Scientific Research, Châtenay-Malabry, France
[c] Université Paris-Saclay, Synchrotron Soleil, 91190 Saint-Aubin, France

Corresponding authors : Dr. Ruxandra Gref: ruxandra.gref@universite-paris-saclay.fr and Prof. Claire Smadja: claire.smadja@universite-paris-saclay.fr

Key words: Protein stability; nanoparticle; PLGA; metal-organic frameworks; synchrotron radiation circular dichroism; capillary electrophoresis, Human Serum Albumin.

Abstract

Nanoparticles (NPs) engineered as drug delivery systems continue to make breakthroughs as they offer numerous advantages over free therapeutics. However, the poor understanding of the interplay between the NPs and biomolecules, especially blood proteins, obstructs NP translation to clinics. Nano-bio interactions determine the NPs' *in vivo* fate, efficacy and immunotoxicity, potentially altering protein function. To fulfill the growing need to investigate nano-bio interactions, this study provides a systematic understanding of two key aspects: i) protein corona (PC) formation and ii) NP-induced modifications on protein's structure and stability. A methodology was developed by combining orthogonal techniques to analyze both quantitative and qualitative aspects of nano-bio interactions, using human serum albumin (HSA) as a model protein. Protein quantification via liquid chromatography-mass spectrometry, and capillary zone electrophoresis (CZE) clarified adsorbed protein quantity and stability. CZE further unveiled qualitative insights into HSA forms (native, glycated HSA and cysteinylated), while synchrotron radiation circular dichroism enabled analyzing HSA's secondary structure and thermal stability. Comparative investigations of NP cores (organic vs hybrid), and shells

(with or without polyethylene glycol (PEG)) revealed pivotal factors influencing nano-bio interactions. Polymeric NPs based on poly(lactic-*co*-glycolic acid) (PLGA) and hybrid NPs based on metal-organic frameworks (nanoMOFs) presented distinct HSA adsorption profiles. PLGA NPs had protein-repelling properties while inducing structural modifications on HSA. In contrast, HSA exhibited a high affinity for nanoMOFs forming a PC altering thereby the protein structure. A shielding effect was gained through PEGylation for both types of NPs, avoiding the PC formation as well as the alteration of unbound HSA structure.

1-Introduction

Engineered nanoparticles (NPs) developed with the advent of nanotechnology hold great promise for revolutionizing medicine owing to their unique physicochemical properties that are different from those of bulk materials. NPs are employed as drug delivery vehicles with targeting and theragnostic abilities [1]. However, the insufficient understanding of NPs' interaction with biological molecules, so-called nano-bio interactions, is an obstacle to their translation into clinics [2].

Immediately after NPs' intravenous administration, a dynamic interplay takes place between their surface and plasma proteins, leading to the formation of a protein corona (PC) [3] [4] [5]. The PC composition depends mainly on the physicochemical properties of the NPs (surface hydrophilicity and charge) and their size and shape [6]. PC governs the biological identity of the NPs and determines their *in vivo* fate, stability, and toxicity [7] [8] [9] [10] [11]. Once adsorbed onto the NPs' surfaces, certain proteins act as opsonins, triggering the recognition and removal of the NPs by the immune system [12].

In most reported studies, the PC formation resulted in a consequent conformational and functional change in the adsorbed proteins [13] [14]. Thus, the nano-bio interactions induced protein structural rearrangements [15] [16] aggregation, inappropriate signaling, and other functional alterations[6] [17] [18]Protein misfolding diseases were attributed to protein unfolding upon nano-bio interactions [19] [20].

Proteins can also interact with NPs, without adsorbing onto their surface. This phenomenon could be related to soft corona formation, where proteins establish weak interactions with NPs and can easily be detached. However, protein contacts with NPs due to Brownian motions can lead to alterations in their structures, but few studies dealt yet with these important aspects. For example, silver NPs of around 15 nm modified the secondary structure of transthyretin, precipitated lysozymes, and affected the stability of human serum albumin (HSA) [21]. Gold NPs denatured bovine serum albumin (BSA) [22] in contrast to Gadolinum-based NPs, which were shown to increase the stability of HSA [23]. Silica NPs of around 26 nm increased the affinity of haemoglobin for oxygen [24]. It was emphasized that the thermodynamic stability and the secondary structure of blood proteins may vary in the presence of NPs [21].

In this context, intensive research was dedicated to engineering the NPs' surfaces to modulate their interactions with proteins, and more particularly, with opsonins [12]. NPs

with protein-repelling surfaces such as those made of poly(ethylene glycol) (PEG) had long blood circulation abilities ("stealth" properties) [25] [1]. PEG is one of the most employed coating materials to reduce protein adsorption onto the NPs. The NPs' surface was successfully engineered with PEG shells by various strategies[26] [27].

There is a clear need of a methodology for the deep understanding of NP interactions with blood proteins, which is crucial to predict their *in vivo* fate and possible toxic side effects. The large majority of analytical methods proposed so far rely on the analysis of the PC: i) sodium dodecyl sulfate–polyacrylamide gel electrophoresis (SDS-PAGE) and mass spectroscopy (MS) allowed protein identification [28]; ii) adsorbed proteins were visualized using optical, electron and atomic force microscopies [29]; iii) the kinetics of protein adsorption were studied by isothermal titration calorimetry (ITC) [20] surface plasmon resonance (SPR) [30] and differential centrifugal sedimentation (DSC) [31]. These techniques give valuable information about the thickness and density of the protein layer on the NPs, the affinity of various proteins for the NPs and the adsorption kinetics. However, they lack structural information on the PC.

In this context, fluorescence spectroscopy has been employed to study protein structure and conformation [32] as well as protein binding affinity for the NPs [33]. However, protein labeling with fluorescent dyes might change their conformation, structure and affinity for the NPs [34]. The strategic combination of different analytical techniques is key in gaining both qualitative and quantitative aspects of the PC and a better understanding of NP-protein interactions [35].

We provide here a comprehensive methodology for the analysis of NP-protein interactions, illustrated in the case of two types of largely investigated NPs (PLGA and nanoMOF) and their PEGylated counterparts, by using HSA as a model protein. Considering NP-serum protein interactions, HSA is typically the first protein to undergo adsorption due to its extraordinary ligand-binding capacity and predominant abundance in the blood. HSA could be a major protein of the inner layer bonding with a high affinity to the particle's surface forming the hard corona [36].

The orthogonal methodology proposed here combines both quantitative and qualitative assessments of the amounts of adsorbed HSA, as well as an evaluation of the integrity of the non-adsorbed protein. Experiments were performed without sample pretreatment to avoid misleading results [37, 38]. First, the amounts of adsorbed HSA were determined by

a BCA test. Subsequently, capillary electrophoresis (CE) was employed to confirm protein adsorption and provide qualitative data on the forms of HSA (native, cysteinated (Cys), and glycated (Gly)) upon contact with NPs. In addition, LC-MS provided quantitative data on the amount of adsorbed protein. Lastly, state-of-the-art Synchrotron radiation circular dichroism (SR-CD) shed light on protein conformation when in contact with the NPs. These orthogonal experiments showed that the two types of NPs (PLGA and nanoMOFs) behaved differently regarding protein adsorption. Surprisingly, in some cases, the protein structure was dramatically altered upon prolonged contact with the NPs even though it was not adsorbed onto them.

2-Materials & Methods

Chemicals

PLGA 50:50 acid terminated (MW: 10–20 KDa, Expansorb® 10P019) and PLGA 50:50 PEG terminated (M_W=32-70 KDa, Expansorb® 10P037) were kindly donated by Sequens (Expansorb®, Aramon, France). Poly (vinyl alcohol) (PVA) (30000-70000 g/mol, 88% hydrolyzed), anhydrous dichloromethane (DCM), sodium chloride (NaCl), sodium phosphate dibasic (Na_2HPO_4), potassium phosphate monobasic (KH_2PO_4), formic acid, 1,3,5-benzenetricarboxylic acid (BTC) and acetonitrile were all purchased from Sigma-Aldrich (Saint-Quentin-Fallavier, France). Iron (III) chloride hexahydrate (98%) was from Alfa Aesar (Schiltigheim, France). Deionized water was obtained from a Direct-QR 3 Water Purification System from Merck Millipore (Billerica, MA, USA). All buffers were prepared using deionized water and filtered through a 0.22 µm nylon (VWR) before use. In particular, phosphate buffer at pH 7.4 (10mM) was prepared by mixing stock solutions of KH_2PO_4 and Na_2HPO_4 in deionized water.

Plasma derived HSA (lyophilized powder, essentially globulin free, ≥99%) was provided by Sigma Aldrich (St. Louis, MO, USA), 4-(2-hydroxyethyl)-1-piperazineethanesulfonic acid (HEPES), sodium phosphate monobasic and sodium dodecyl sulfate (SDS) were obtained from Thermo Fisher Scientific (Les Ulis, France). The background electrolyte (BGE) used in CZE was 75 mM HEPES, containing 0.5 mM SDS at pH 8.0 adjusted with 1 M NaOH before adding water to a final volume of 50 mL. Pierce™ Bicinchoninic acid (BCA) protein assay kit was purchased from Thermo Fisher Scientific.

Preparation of PLGA and PLGA-PEG NPs

PLGA NPs were prepared as previously reported using PVA as an emulsifier and using 1 mL DCM solutions of PLGA or PLGA-PEG (75 mg/mL) [38] as the organic phase. Briefly, aqueous and organic phases were mixed using a sonic probe (Sonopuls HD 2070, BANDELIN electronic GmbH & Co, Berlin, Germany) at 40% of power for 15s. The dispersion medium was 5 mL of 0.5% *w/v* PVA solution containing 1% w/v NaCl and was sonicated for 30s at 40% power in an ice bath to avoid overheating. The resulting emulsion was left at room temperature under gentle magnetic stirring overnight to allow the organic solvent to evaporate.

Synthesis of CD-PEG derivative

CD-PEG was synthesized as previously described using phosphorylated β-cyclodextrin (β-CD) building-blocks to bind to the metallic sites on the nanoMOF surface[26]. β-CD was chosen because its dimensions are, as needed, large enough to avoid penetration within the MIL-100(Fe) nanoMOFs pores, and their numerous free OH groups are suitable for introducing functional groups in the primary or/and secondary rims. Briefly, 1-azido-1-deoxy-ω-O-methoxypentatetraconta(ethylene glycol) was firstly synthesized followed by coupling to phosphorylated CD to yield Heptakis {2,3-di-O-{10-[methoxypentatetraconta (ethylene glycol)yl-1H-1,2,3-triazol-40-yl]- methyl}} cyclomaltoheptaose phosphate sodium salt, abbreviated here CD-PEG. It was characterized by ^{1}H-RMN (600 MHz, D_2O) and high-resolution inductively coupled plasma mass spectrometry (HR-ICP-MS) to determine the composition and amounts of key elements (P 8.0%).

Synthesis of MIL-100(Fe) nanoMOF and PEG coating

Iron trimesate nanoMOFs were synthesized using a microwave-assisted hydrothermal method described elsewhere [27] [39]. Briefly, 30 mL of an aqueous mixture containing 6.0 mM iron chloride hexahydrate and 4.0 mM of BTC was heated at 130°C under stirring for 6 min and under microwave irradiation at 1600 W (Mars-5, CEM Corporation, Matthews, NC, USA). The synthesized nanoMOFs were recovered by centrifugation at 10000 g for 15 min and purified by six times washing with absolute ethanol. They were stored as ethanolic suspensions at room temperature until further use. Before the experiments, ethanol was removed by centrifugation and nanoMOFs were redispersed in aqueous media by vortex.

PEG-coated nanoMOFs (nanoMOFs-PEG) were prepared as previously reported[40] [26] by incubating overnight at room temperature the nanoMOFs suspensions in water (2mg/mL) with CD-PEG solutions (0.2 mg/mL).

NP characterization

The morphology of NPs was visualized by transmission electron microscopy (TEM) with a JEOL electron microscope (JEM 100 CX II, operating at 120 kV) equipped with a US1000 2kx2k Gatan camera. 5 µL of samples were deposited onto a carbon-coated copper grid treated beforehand with a glow discharge (easiGlow, Ted Pella Inc), and excess liquid was removed with a filter paper after 30s.

Mean hydrodynamic diameters and size distributions were determined by dynamic light scattering (DLS) at 25°C with an equilibration time of 60s using a Zetasizer® (Nano ZS90, Malvern Instruments, Worcestershire, UK). All formulations were measured at least in triplicate. Mean diameters were reported as Z Average (nm) ± SE (Standard Error) with the polydispersity index (PdI). Zeta potential (ZP) was measured in KCl 1 mM at 25°C with a Zetasizer®. Additionally, the porosity of nanoMOFs was characterized by nitrogen sorption measurements performed on Micromeritics Instruments ASAP 2020 at 77 K. Samples were degassed at 100 °C for 15 h. BET surface area of 1690 ± 80 m^2 g^{-1} was obtained by calculating in the partial pressure range of 0.05 – 0.20 P/P_0. NanoMOF-PEG samples were prepared as previously described by incubation with an aqueous solution of CD-PEG overnight [26]. After surface functionalization, the nanoMOF-PEG was recovered by centrifugation (10 min, 10000 g). The crystallinity of the nanoMOFs was preserved before after surface modification with CD-PEG, as assessed by X-ray powder diffraction (XRPD) in agreement with previous investigations [26].

HSA adsorption studies

PLGA and PLGA-PEG NPs (3 and 10 mg/mL) were incubated with HSA (1 mg/mL) in phosphate buffer (0.01M, pH 7.4). NanoMOF and nanoMOF-CD-PEG (1.5 or 3 mg/mL) were incubated with HSA solutions (0.5 or 1 mg/mL). In all cases, the HSA:NP weight ratio was 1:3. All NPs were dispersed in 300 µL phosphate buffer (0.01 M, pH 7.4) and were incubated at room temperature up to 72 h using a vertical rotating shaker. In all cases, the unbound HSA was assessed in the supernatants obtained after NP centrifugation at 10,000 g for 15 min.

Quantification of protein adsorption at the surface of NPs : Bicinchoninic acid (BCA) assay

The HSA adsorption kinetics were studied by monitoring the unbound HSA concentration as a function of time. The unbound protein concentration was determined colorimetrically with a Pierce™ BCA protein assay kit. To do so, 25 µL of supernatants containing the unbound proteins were recovered after NP centrifugation and were mixed with 200 µL of the BCA reagent in a 96-well microplate. The samples were well shaken and incubated at 37 °C for 30 minutes. After cooling for 15 minutes, the absorbance was read at 562 nm using a microplate reader (Infinite 200, Tecan Inc., Switzerland). The amount of unbound protein was calculated by interpolation of a calibration curve using HSA standards with known concentrations. Controls were aqueous solutions and NP suspensions without HSA. The results were reported as the mean value of at least three separate experiments.

Capillary zone electrophoresis coupled to UV (CZE-UV)

CE experiments were performed on a P/ACE MDQ Instrument (Sciex, Framingham, MA, USA), coupled to a diode array detection UV-vis detector that was set at 214 nm. The 32 KaratTM software version 7.0 (Sciex) was used to collect data. The analysis was carried out by using PVA-coated capillaries, purchased from Sciex, with an internal diameter of 50 µm and a total length of 60.2 cm (effective length of 50 cm). Before the first use, the PVA capillaries were rinsed at 30 psi for 10 min with water and freshly prepared BGE (75 mM HEPES containing 0.5 mM SDS at pH 8). The sample was hydrodynamically injected from the inlet by applying a pressure of 0.5 psi for 15 s. The separation was then conducted at −25 kV at 25 °C. Between each analysis, the capillary was flushed at 20 psi for 15 min with water and 15 min with BGE. At the end of the day, the capillary was rinsed with water (15 min, 20 psi) and BGE (15 min, 20 psi) and stored at 4 °C with the ends in water as previously described [41].

Liquid Chromatography-Tandem Mass Spectrometry (LC-MS/MS)

Unbound HSA was analyzed with a Waters Xevo G2-XS QTof/Tof - ACQUITY UPLC M-Class system run by Masslynx v4.1 (Waters) after dilution in water with 0.1% (v/v) formic acid to reach a final concentration of 0.01 mg/mL. Samples of 1 µL were loaded onto a C18 trap column (NanoE MZ Sym C18 5µm 180um x 20 mm, Waters), at 20 µL min^{-1} and desalted with 0.1% (v/v) formic acid and 5% (v/v) acetonitrile. After 4 min, the precolumn was connected to C18 Nanocolumn (NanoE MZ PST CSH130, 1.7µ 75µm x 150 mm, Waters).

Electrospray ionization was performed at 2.5 kV, with a source temperature of 120°C, desolvation temperature of 250°C and 80 L/h cone gas flow. Buffers were 0.1% formic acid in water (A) and 0.1% formic acid in acetonitrile (B). Peptides were separated using a linear gradient from 5 to 95% buffer B for 80 min at 300 nL min^{-1}. One run was performed in 90 min, including the regeneration step at 95% buffer B and the equilibration step at 95% buffer A.

Mass spectrometric data were investigated with the Masslynx v4.1 software (Waters). Background subtraction was applied to mass spectrum with polynomial order at 25, below curve at 5%, tolerance at 0.01. Deconvolution was run on the 6 most intense peaks by Max Ent1 function by iteration to convergence with the following parameters: output mass ranges 60000-70000 Da with resolution 1.00 Da/channel, damage model as uniform Gaussian with at half height of 1.00 Da.

SRCD

The SRCD measurements were performed at the DISCO-beamline, SOLEIL Synchrotron (Saint-Aubin, France). Thanks to the photon flux and beam size at the Synchrotron facility, the measurements were performed with a good signal-to-noise ratio (200) down to 175 nm, which is difficult to reach with a conventional CD set-up. Thus, the UV CD region (175–250 nm) corresponding to peptide bond absorption was analyzed using the DISCO SRCD set up. Spectra were acquired every nanometer using a 1 nm bandwidth and 1.2 s integration time. Raw data (θ) was measured in millidegrees (mdeg), which were converted to molar circular dichroism values (Δε), after averaging, baseline subtraction and calibration with (+)-camphor-10-sulfonic acid (CSA). Data treatment including average, baseline subtraction, smoothing, scaling and standardization was performed with the CDtool software [42].

For the molar circular dichroism values or Δε, the following equation was applied:

$$\Delta\varepsilon=\theta\times(0.1\times MRW) / [(P\times C)\times 3298] \quad (I)$$

The mean residue weight (MRW) of HSA is 113.8 Da (g.mol^{-1}), pathlength (P) is 0.00234 cm (measured by interferometry) [42] and protein concentration (C) is 1 mg/mL.

The secondary structure content was determined by using ContinLL and SELCON3 programs [42] and additionally BeStSel server [43]. Normalized root-mean-square deviation (NRMSD) indicated the most accurate fit for each spectrum.

The NP suspensions after their incubation with HSA were analyzed directly without separation of the unbounded protein. To do so, 4 µL samples were loaded in circular demountable calcium fluoride cells with a path length of 50 µm [44]. Baselines were collected in triplicate for all samples, corresponding to buffer solutions, suspension media or NP suspensions without protein.

Thermal denaturation experiments were carried out by collecting SRCD spectra at temperatures ranging from 23 to 98 °C using a 3 °C step and a 5 min settling time. Three spectra were collected for each temperature with a total measurement time of 3 h. Spectral cut-off at 180nm was used, based on the high tension of the PMT (Photomultiplier Tube) corresponding to an absorbance below 1. As controls, spectra were also recorded for 3 h without changing the temperature to ensure that over this time, no additional phenomena (radiation damage or drying) affected the spectral amplitude. These controls showed that HSA was not susceptible to radiation damage and that the photon flux and beam size were appropriate for the investigations [45], [46].

4-Results and discussion

4.1-Preparation of the NPs

Firstly, PLGA and PLGA-PEG NPs were prepared using commercially available biodegradable polymers [38]. While the hydrophobic PLGA polymer possesses carboxyl end groups, the PLGA-PEG diblock copolymer is uncharged. The hydrophilic PEG units covalently attached to the PLGA block dispose in a "brush" conformation at the NPs' surface leading to protein-repellent surface properties [47]. Both PLGA and PLGA-PEG NPs were prepared by using an emulsifier, PVA, that forms a neutral, hydrophilic shell on the surface of the NPs, as it has been previously described [48]. For over 25 years, the versatile NPs of PLGA and PLGA-PEG have been utilized to encapsulate and deliver in a controlled manner a wide range of hydrophilic and hydrophobic drugs [49].

Secondly, biodegradable MIL-100(Fe) nanoMOFs were synthesized by a "green" (organic solvent-free) microwave-assisted hydrothermal method generating an open 3D porous crystalline architecture. The nanoMOFs possess mesoporous windows (5.6 and 8.6 Å) and internal cages of around 24 and 29 Å in diameter [50]. Discovered more recently than the polymeric PLGA and PLGA-PEG NPs, they have the advantage of being able to incorporate a variety of drugs without the use of organic solvents reaching payloads up to 20–70 wt% [50] and were well tolerated *in vivo* [51].

Aiming to develop biomedical applications of nanoMOFs, some of us have set up strategies to modify the nanoMOFs' surfaces with PEG chains by mild, one-step procedures devoid of reactants and organic solvents[26] [27]. The coating was based on cyclodextrin (CD) derivatives that are large enough to avoid their penetration within the nanoMOF's pores, and not to interfere with and displace the loaded drugs [27]. The CD scaffolds displaying grafted PEG moieties (average MW ~2000 g/mole) spontaneously adsorbed onto the nanoMOFs, where they are firmly anchored by coordination with the available metal sites at the surface [26]. Advantageously, the procedure was carried out in a one-step procedure in water and without using any toxic additives and led to stable coatings without altering the nanoMOFs' crystalline structure.

4.2-Morphology and characteristics of NPs

PLGA and nanoMOF NPs, PEGylated or not, were successfully prepared with similar sizes to allow a comparative study of their nano-bio interactions as a function of both their core and surface properties **Fig. 1A-D**). Whereas the PLGA NPs appeared round-shaped, the nanoMOFs were crystalline with facetted structures in agreement with previous studies [40] [26]. In all cases, the average diameters ranged from 80 to 370 nm. These sizes were in agreement with DLS measurements, which showed that the PLGA and nanoMOFs NPs had mean hydrodynamic diameters of 310 ± 15 and 234 ± 16 nm, respectively (Table 1, SI). The polydispersity indexes (PDIs) were respectively 0.1 and 0.2, indicating that the NPs were monodisperse. PLGA-PEG and nanoMOF-PEG NPs had larger diameters of 418 ± 30, and 286 ± 20 nm, respectively.

The Zeta potential for PLGA and PLGA-PEG NPs was around 0 mV, attributed to their neutral PVA shell, as previously reported [48]. This protective steric layer shields the negative charges of the carboxyl end group of PLGA. The nanoMOFs, coated or not, had Zeta potentials of -17±3 mV, in good agreement with previously published data[40] [26].

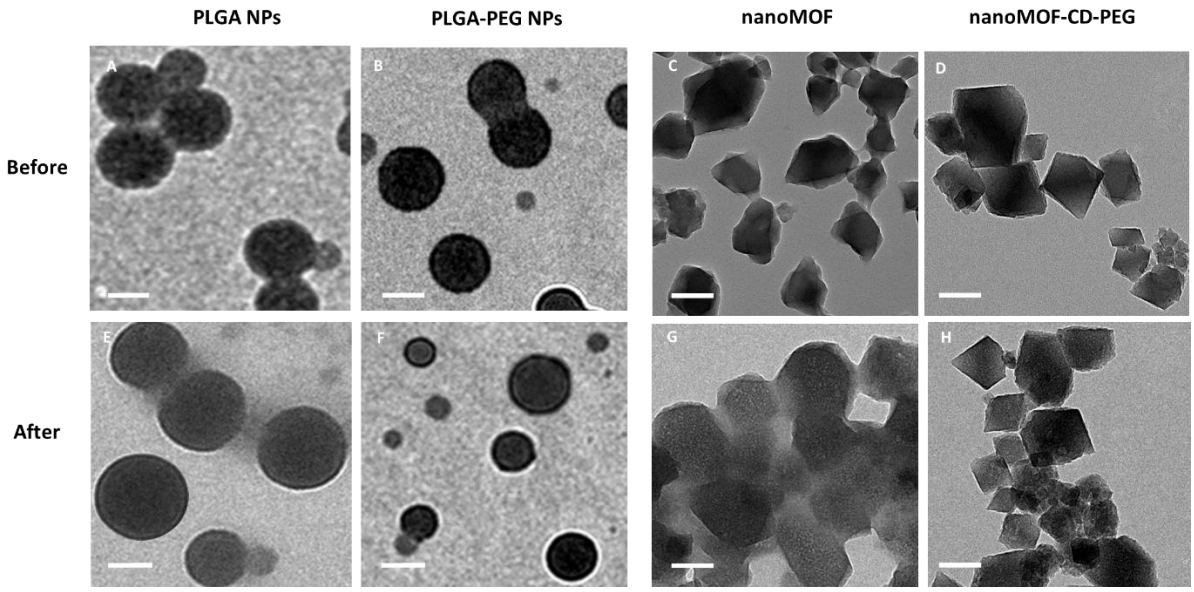

Fig. 1. Representative TEM images of: A) PLGA NPs; B) PLGA-PEG NPs; C) nanoMOF and D) nanoMOF-PEG. TEM images obtained after incubation with HSA: E) and F) PLGA and PLGA-PEG NPs, after three days (1:10, HSA:NP); G) and H) nanoMOF and nanoMOF- PEG after 2h (1:3, HSA:NP). Scale bars: 100 nm.

4.3-Nano-bio interactions

Kinetics of protein adsorption

The kinetics of HSA adsorption onto the two types of NPs, hybrid and polymeric, with different core and shells, were compared. The NPs were incubated with HSA solutions and incubated up to 24 h. The unbounded HSA was quantified using a BCA colorimetric assay at different time intervals (**Fig. 2)**.

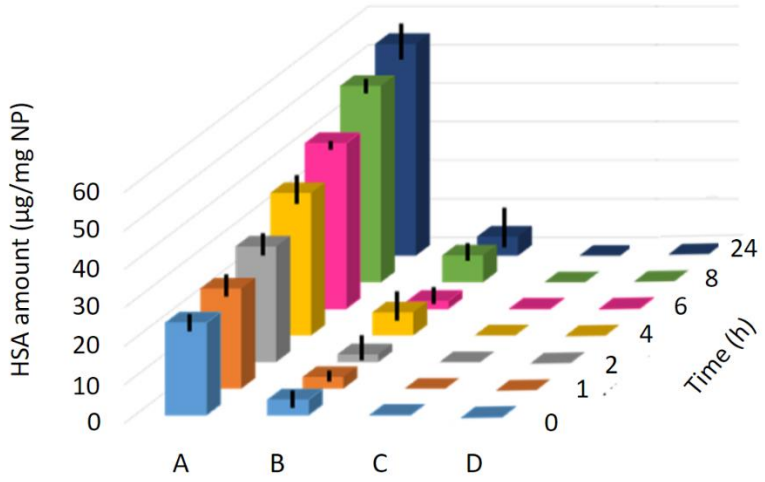

Fig. 2: Amounts of HSA (µg/mg of NPs) adsorbed on nanoMOFs (A), nanoMOFs-PEG (B), and PLGA NPs coated or not with PEG (C). The HSA:NP weight ratio was 1:3 for the nanoMOFs and nanoMOFs-PEG, and 1:3, 1:10 and 1:100 for the PLGA and PLGA-PEG NPs. Different time points were studied: 5 min (light blue); 1 h (orange); 2 h (grey); 4 h (yellow); 6 h (pink); 8 h (green) and 24 h dark blue).

For nanoMOFs, HSA adsorption occurred as soon as they were in contact with HSA (amount of adsorbed proteins 24±2 µg/mg, 5min). Then, HSA adsorption gradually increased in a time-dependent manner up to around 55 µg/mg until a plateau is reached at the 8th hour of incubation **(Fig. 2).** In contrast, the amount of adsorbed HSA was very low in the case of nanoMOF-PEG (less than 7±2 µg/mg) regardless the incubation time. This suggests that the affinity of HSA for the nanoMOF surface decreased while they gained "stealth" properties through PEGylation.

Surprisingly, neither the PLGA nor the PLGA-PEG NPs did adsorb any significant protein amounts. Even within three days of incubation, the adsorbed amounts were undetectable by the BCA assay. This was the case also when increasing the HSA-NP contact area (i.e. decreasing the HSA:NP ratio to 1:10 and 1:100). Taking into account the surface area developed by the NPs, it was calculated that less than 0.15 mg/m^2 HSA was adsorbed. Therefore, it was concluded that the affinity of HSA for both PLGA and PLGA-PEG NPs was very low as compared to bare and PEGylated nanoMOFs.

The striking differences in protein adsorption between the two types of analyzed NPs could be explained based on their composition and physicochemical properties such as surface charge and hydrophilicity. PLGA NPs possess a neutral and hydrophilic surface in reason of their PVA coatings [35]. In contrast, the bare surface of the nanoMOFs is negatively charged and displays numerous accessible iron sites prone to bind large molecules such as proteins [52]. In addition, despite its global negative charge at pH 7.4 (pI 4.7), HSA-positive residues could interact with the negative charges of the nanoMOFs. Whatever the NPs (PLGA or nanoMOF), the PEG shells protected them against protein adsorption.

Finally, the kinetic studies performed here provided the incubation conditions to be carried on for the following PC investigations in phosphate buffer. In the case of nanoMOFs, two hours were sufficient to form a large PC without NP degradation [53]. Indeed, nanoMOFs progressively degrade in phosphate buffer, losing their organic linkers

and forming amorphous structures [53] [54]. In contrast, PLGA formulations were stable in phosphate buffer, so they were studied over three days in this medium.

NP morphology upon contact with protein

NP morphologies were investigated after incubation with HSA by TEM (**Fig. 1E-H**). The micrographs revealed that both PLGA and PLGA-PEG NPs maintained their uniform and spherical shapes and the images were similar to the prepared NPs (**Fig. 1A-B**). Both PLGA and PLGA-PEG NPs preserved their morphology after contact with HSA for 3 days with no evidence of PC formation (**Fig. 1 E**-**F**), in line with the HSA kinetic findings (**Fig. 2**), which demonstrated no HSA adsorption onto the polymeric NPs.

On the other hand, TEM images showed that the facetted morphology of nanoMOFs and nanoMOF-PEG were preserved after interaction with HSA (**Fig. 1G-H**). Noticeably, only uncoated nanoMOFs after incubation with HSA presented a blurry aspect (**Fig. 1G**), not observed with PEG-coated ones (**Fig. 1H**). Given the high HSA adsorption onto these NPs **(Fig. 2)**, it's plausible to hypothesize that this blurry aspect is due to the formation of a PC.

To investigate in depth the ~~corona formation~~ impact of the interaction with NPs for proteins. Capillary zone electrophoresis has been chosen as this method allows; (i) the analysis of unbound HSA, (ii) the evaluation of the impact on different forms of HSA (native, cysteinylated, or glycated). This versatile technique also brings insights into the possible alterations of the unbound HSA after contact with the different NPs studied here.

CZE

CZE is a versatile method allowing the investigation of HSA behavior on NPs by both quantitative and qualitative approaches [55] [56] [57] [58] [59]. For this study, PVA-coated capillary has been employed considering its excellent ability to separate different forms of HSA: native, glycated, and cysteinylated [44].

Bar-Or and his coworkers highlighted the heterogeneity of albumin by liquid chromatography coupled with mass spectrometry[60]. Several HSA isoforms have been found, among them native HSA, cysteinylated HSA, and glycated forms [60]. Glycated HSA is an additional clinical marker to monitor blood glycemia, and cysteinylated HSA is a key plasma marker of oxidative stress [61]. In the above-mentioned studies [44], the analysis of the protein peak area will provide quantitative information on protein adsorption.

Therefore, potential modifications on the relative amounts of the different unbound HSA forms can be evaluated qualitatively to gain more detail on HSA interactions with NP surfaces [57]. Therefore, CZE was a method of choice here to investigate nano-bio interactions combining both quantitative and qualitative aspects.

Therefore, the NP series (nanoMOF and PLGA) were then incubated with HSA and their supernatants were collected to investigate the aforementioned two aspects: i) quantitative by analyzing the peak areas of unbound HSA and ii) qualitative by analyzing potential peaks modification for the three HSA forms (native, cysteinylated, and Glycated). **Fig. 3** presents the CE-UV profiles of HSA recovered from NP supernatants after the incubation studies. First, CE experiments were performed on HSA solutions (without NPs) to investigate the stability of the protein in the experimental conditions employed here for adsorption studies. Thus, the HSA solutions were incubated for up to three days at RT or 37°C and were subjected to the centrifugation conditions employed to sediment the NPs (without any NPs in the medium). The CZE electropherograms were then compared to those of fresh HSA solutions **(Fig. SI1)**. The electrophoretic profiles of the HSA solutions remained unaltered whatever the experimental conditions, pointing out the stability of HSA under the experimental conditions used here to study its interaction with the NPs. Indeed, when reference HSA is incubated without any NPs, three reproducible peaks at 12.4, 12.5 and 12.7 min were obtained. These data are in agreement with previous studies using the same type of capillaries which showed the three HSA peaks assigned to Glycated, native and Cysteinylated forms, respectively [41].

Then, the interactions between PLGA and PLGA-PEG NPs and HSA were investigated. CE profiles of unbound HSA obtained after incubation with PLGA and PLGA-PEG NPs at an HSA: NP ratio of 1:3 (**Fig. 3A,** blue and orange lines) were almost identical to the control HSA (not incubated with NPs). However, an increase in the NP concentration from 3 to 10 mg/mL (ratio 1 :10) resulted in a significant decrease of the peak at 12.7 min corresponding to the Cysteinylated HSA. Moreover, a new peak appeared at 11.8 min for this ratio. Interestingly, the total area of all the HSA peaks remained similar to the reference, with differences of less than 5%. It is worth mentioning that identical CZE profiles were obtained when PLGA and PLGA-PEG NPs were incubated with HSA for either one (**Fig. SI2**) or three days (**Fig. 3A**) whatever the ratio of HSA: NPs. In contrast, when the incubation time was limited to 2h, there were no significant modifications in the HSA profile even at the HSA:

NP ratio of 1:10 (**Fig. SI3**). This shows the dependence of the qualitative aspect of nano-bio interactions on both concentration and incubation time.

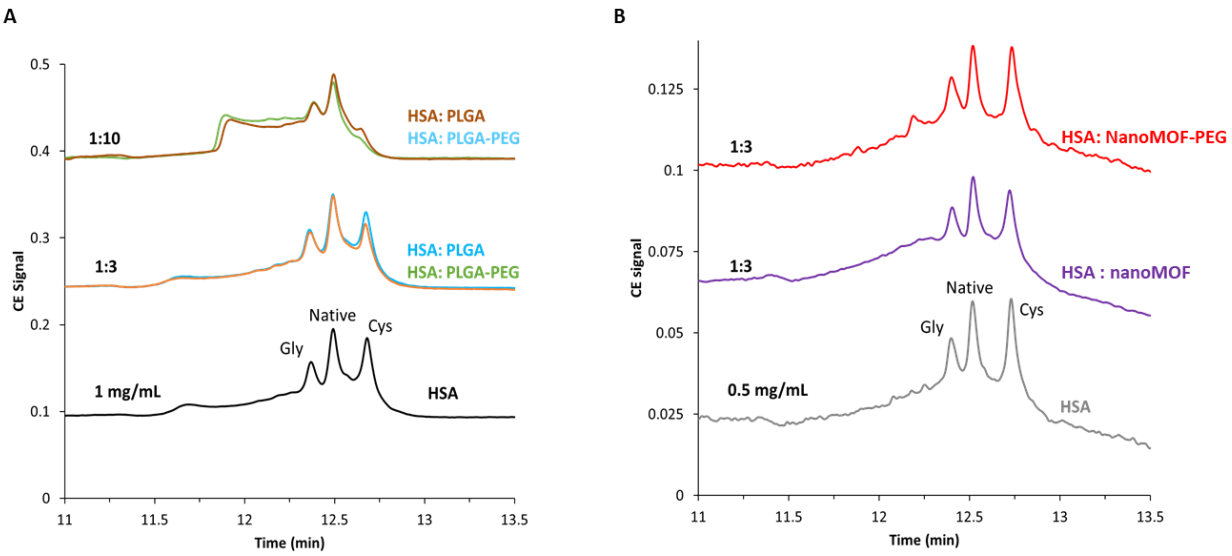

Fig. 3: CE-UV electropherograms of unbounded HSA recovered from supernatants after incubation with A) PLGA-PEG (green, orange) and PLGA (brown, blue) NPs during 3 days with HSA: NP ratio of 1:3 and 1:10. B) nanoMOF-PEG (red) and nanoMOF (purple) during 2h with HSA: NP ratio of 1:3. Black and grey lines are the reference HSA solutions at 1 and 0.5 mg/mL, respectively.

Thus, we speculate that the shift of Cysteinylated HSA might correspond to a structural alteration of the protein, although it did not adsorb onto the NPs' surfaces (**Fig. 2**). These findings suggest that HSA in contact with PLGA-based NPs might undergo structural modifications despite their low affinity towards them. As shown here, these modifications could be observed whatever the incubation time and NP concentration (i.e. developed surface areas). Therefore, the next step was dedicated to the interactions between HSA and nanoMOFs. Indeed, it was then interesting to investigate if structural changes occur with HSA upon incubation with nanoMOFs, where important amounts (30 ±2 µg/mg) were adsorbed within 2h **(Fig. 2)**. For nanoMOFs with higher affinity for HSA, no modification of the HSA profile (ie no change of the retention times) was observed on the unbound HSA species after incubation **(Fig. 3B)**. However, the 11±3% decrease in the peak area after incubation with the nanoMOF is an indication that around 37±9 µg of the HSA was

adsorbed per mg of nanoMOF, which is in a good agreement with the BCA protein assay (30 ±2 µg/mg adsorption, **Fig. 2**). Moreover, the shielding effect gained through PEGylation was evident as the area of unbound HSA remained unchanged after incubation with nanoMOF-PEG (less than 5 % changes) compared to reference HSA. To conclude, we can observe from these experiments that HSA was able to adsorb only on non-PEGylated nanoMOFs NP surfaces but did not bind nanoMFs-PEG, nor PLGA NPs (coated or not with PEG). However, we observed for PLGA NPs (coated or non-coated with PEG) a decrease of the peak area corresponding to cysteinylated forms, whereas the total of all HSA peak areas remains similar to the reference, thereby suggesting a possible conformational modification. To the best of our knowledge, no study has yet reported potential conformational modification for HSA forms upon incubation with NPs. However, more detailed investigations would be needed to explain the observations concerning the Cysteinylated forms after incubation with PLGA NPs.

In complement to the CZE studies, LC-MS investigations were carried on in an attempt to resolve the HSA forms in the NP supernatants.

LC-MS investigations

Total ion count (TIC) chromatograms provided in **Fig. 4** represent the ion intensities displayed as a sum of the individual HSA fragments as a function of incubation time with the PLGA NPs and nanoMOFs, PEGylated or not. The incubation time was 72h for PLGA and 2h for nanoMOFs. TIC chromatograms of unbound HSA after incubation with or without NPs revealed similar shapes and same retention time (75.2 min) in all the studied cases (**Fig. 4).** When HSA was incubated with PLGA and PLGA-PEG NPs, an additional small peak appeared at 74.7 min. It corresponds to free PVA emulsifier in the NP suspensions, and it induced no effect on the main peak (**Fig. 4B-C)**.

Values derived from the areas under the intensity curves give insights about the abundance of the protein thus relative protein quantity between samples. As indicated next to the chromatograms in **Fig. 4A-B**, areas under the curve values did not vary between incubated HSA reference and HSA in contact with PLGA (<14% deviations in the areas). Therefore, it is in agreement with the quantitative BCA assay findings, which showed that HSA was not adsorbed on the PLGA NPs. In contrast, a dramatic change was recorded when HSA was in contact with nanoMOFs (non-PEGylated): 50% of reduction occurred in comparison to incubated HSA reference **(Fig. 4D-E)**. This observation aligns

with the previously mentioned findings, which suggest a decrease in unbound HSA in the supernatant, thereby indicating the formation of a PC. Interestingly, PEGylated NPs, namely PLGA-PEG and nanoMOF-PEG, demonstrated a clear resistance to protein adsorption. This was evidenced by the minimal differences of 12% and 4% respectively, when compared to the HSA reference. **(Fig. 4E-F)**.

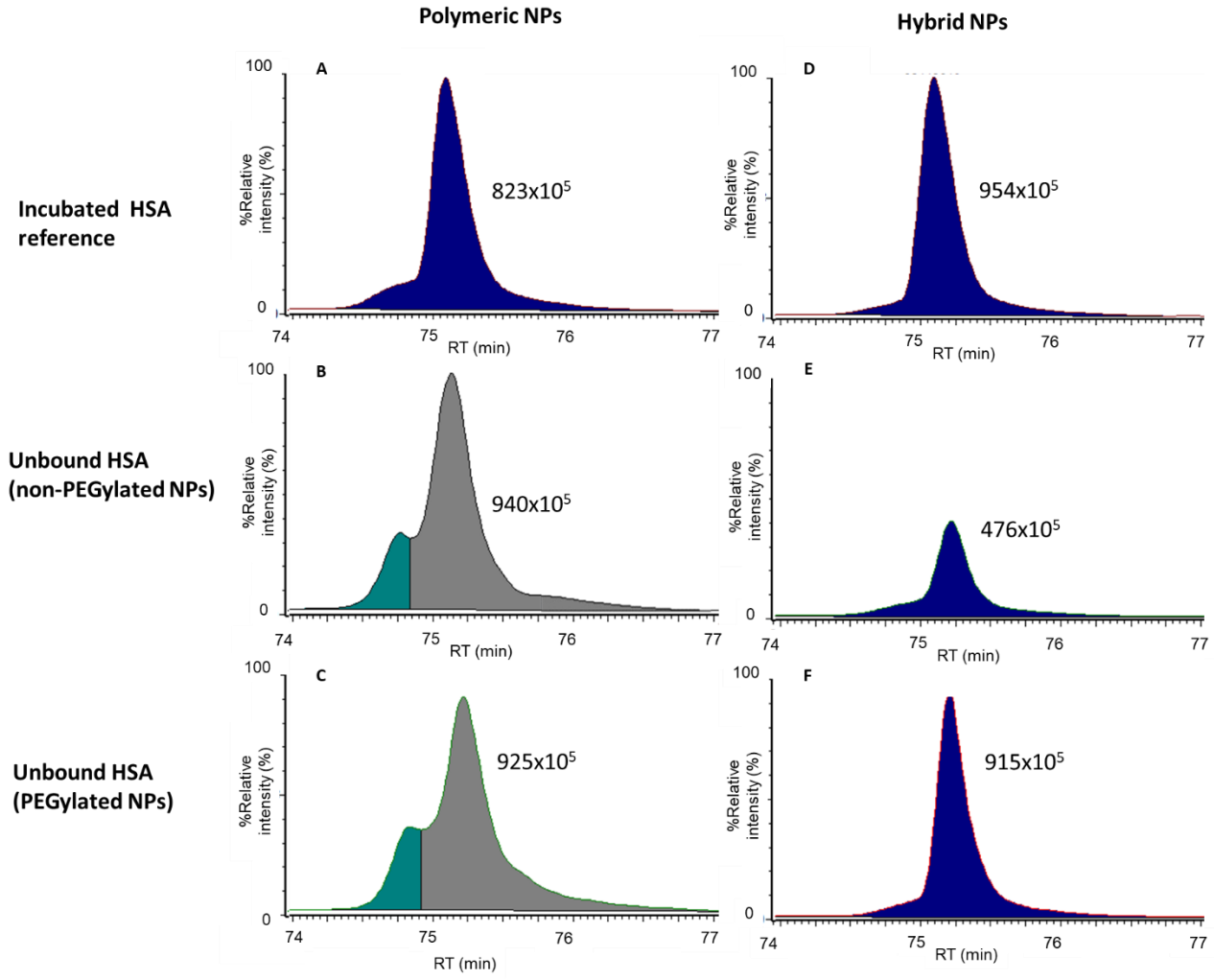

Fig. 4. TIC chromatograms of unbound HSA recovered after the incubation A) without NPs, for 3 days B) with PLGA NPs, for 3 days, C) with PLGA-PEG NPs, for 3 days, D) without NPs, for 2h E) with nanoMOF for 2h, F) with nanoMOF-PEG for 2h.

SR-CD investigations

To complete these studies, SR-CD was a method of choice to investigate the changes in the secondary structure of the HSA protein due to its interaction with the NPs. The CD provides access to the relative content of the secondary structure components of HSA (alpha-helix, beta-sheet, beta-turns, and random coil). While the extended spectral range was reached from 175 to 250 nm using synchrotron radiation in the DISCO beamline, the entire protein peak at 192 nm was recorded which is of interest regarding the singlet electron transitions in the HSA peptide backbone **Fig. 5.** We can observe from **Fig. 5**, that HSA exhibited a typical spectrum of a predominantly α-helical protein with two minimums at 224 and 208 nm and a maximum at 192 nm. These data were in agreement with the literature [50]. The peak at 224 nm was attributed to the nπ* transition from the lone pair of oxygen to a π* anti-bonding orbital. The peak observed at 208 nm was due to the ππ* electronic transitions of the peptide bond, whereas a positive band at 192 nm was due to the transition of non-bonding π orbital to the π* orbital [62]. The region around 180 nm is known as a charge transfer region. Unlike other transitions, the transitions in this region occur intramolecularly from one peptide bond to another [63].

The amount of α-helical secondary structure of HSA was obtained by deconvolution of the CD spectra. Fresh HSA reference used here presented a 70% helix content which was in agreement with the literature [64]. This helicity content was preserved 2h after incubation (70%), whereas it dropped to 61% after three days of incubation **(Fig. 5A)**. The decrease in the HSA helicity upon incubation has been shown in various studies based on CD spectroscopy, confirming the results found here [65] [66].

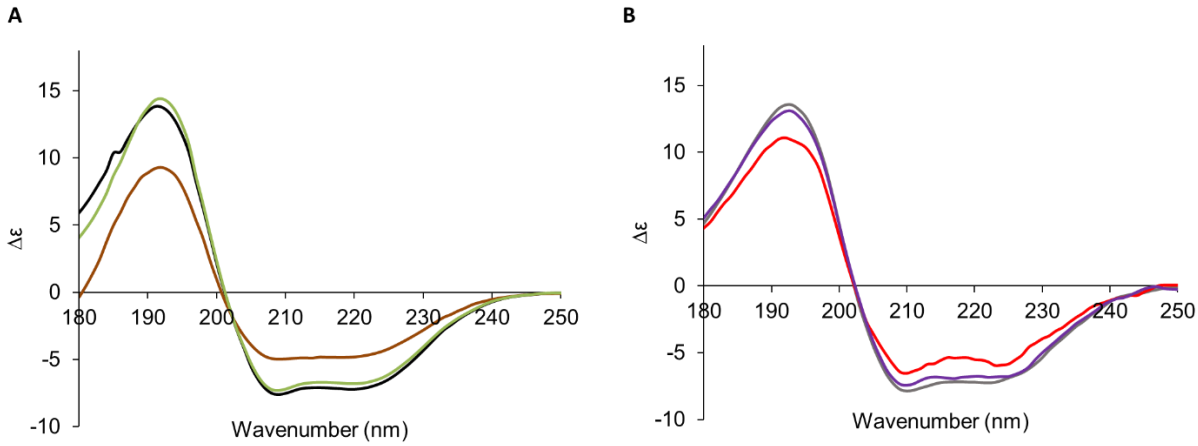

Fig. 5 Far UV SR-CD spectra of : control HSA incubated during 2h (grey) and 3 days (black); **A)** PLGA: PLGA (brown) and PLGA-PEG (green) NPs incubated with HSA during 3 days at a HSA: NP ratio of 1:10; **B)** nanoMOF (purple) and nanoMOF-PEG (red) incubated with HSA during 2h at a HSA: NP ratio of 1:3. The spectra were taken directly on the NP suspensions and in all studies, the concentration of HSA was 1 mg/mL.

The interactions of bare and PEGylated NPs with HSA were analyzed by SR-CD directly on the NP suspensions as the NPs did not interfere with the experiments **(Fig. 5)**. A special attention was given to HSA secondary structure differences between the reference (HSA incubated without NPs) and HSA in the presence of the four types on NPs. Firstly, the contact of HSA with the PLGA NPs for 3 days (1:10, HSA: PLGA NP) resulted in a dramatic loss in α-helix content (from 61 to 27%) with visible signs of modifications that affected the bands at 224 nm (nπ* parallel transitions), 208 nm (ππ* parallel transitions) as well as at 192 nm (ππ* perpendicular transitions) **(Fig. 5A)**. A significant change observed around 180 nm indicated that HSA was subjected to intramolecular charge-charge transitions. On the other hand, the increase recorded on HSA's parallel β-strand (from 0 to 4%) and antiparallel β-strand (from 0 to 12%) signified the increase in β-sheet populations. Possibly, a minor denaturation or reorganization with the formation of β-strands took place during collisions at the NPs' surfaces, without leading to adsorption as it was previously established **(Fig. 2)**. Noticeably, when lower quantities of PLGA and PLGA-PEG NPs were in contact with the same amount of HSA, the α-helix structure of the protein remained unaltered confirming the concentration dependence of the nano-bio interactions (**Fig. SI4**).

HSA incubated (2h) with nanoMOFs was then analyzed and compared with incubated (2h) HSA reference **(Fig. 5B)**. After contact with NPs, a loss in α-helix content of HSA was observed, from 70% to 52 %. This decrease was remarkable taking into account the short incubation time of only 2h. Further analysis of the SR-CD data showed only a slight increase in antiparallel β-strands (from 0 to 2%) and in beta-turns (from 9 to 14%). Besides, the percentage of other secondary structure components (unordered) increased from 21 to 32%.

Conversely, the CD spectra in the case of HSA incubated with PLGA-PEG NPs and nanoMOF-PEG were similar to their reference HSA spectra (**Fig. 5**). The α-helix content was preserved with less than 5% differences (within the detection limit of the method) as compared to control HSA.

In a nutshell, these results suggest that the PEGylated surfaces preserve the α-helix structure of the protein, whereas uncoated surfaces disturb it regardless of whether adsorption has taken place or not.

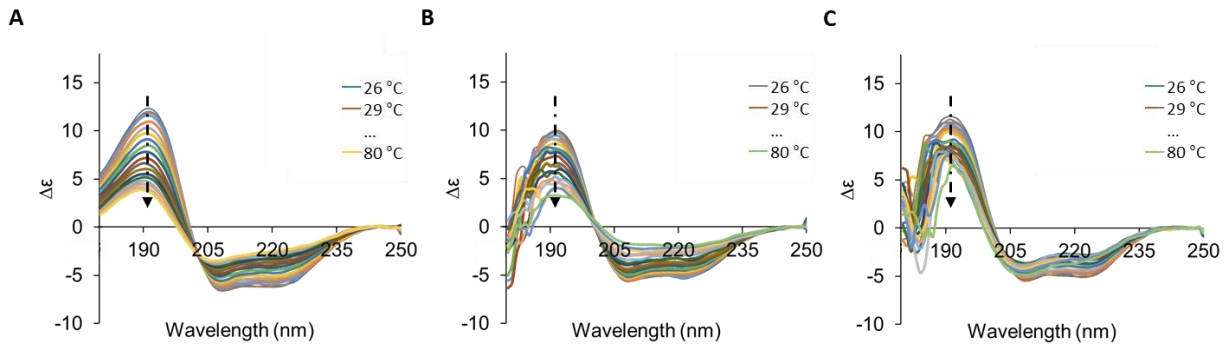

Fig. 6. Thermal unfolding of HSA followed by SR-CD spectroscopy as a function of temperature over a range from 26 to 80°C at intervals of 3 °C. **A**) incubated HSA reference (1mg/mL), **B**) HSA: PLGA NPs (HSA: NP ratio of 1:10), **C**) HSA: PLGA-PEG NPs (HSA: NP ratio of 1:10). The samples were analyzed after 3 days incubation.

To go a step further, protein unfolding was analyzed through thermal denaturation studies that give insights into the effect of NPs on protein's thermal stability. Far-UV SRCD spectra were collected over a wide temperature range, from 26 to 80 °C. **Fig. 6A** shows a typical spectrum of HSA unfolding upon an increase in temperature. All the thermal unfolding spectra intersected at 203 nm which corresponds to the isosbestic point. The HSA thermal unfolding was then assessed after incubation with the NPs. The changes in the unfolding behavior of HSA due to interactions with the PLGA NPs are presented in **Fig. 6B**. The isosbestic point was shifted from 203 nm to 201 nm, which is a clear indication of a reduction in HSA's stability.

In addition, changes in other spectral features were also noted. The spectra from the first scan appeared to be in a less compact state compared to the reference HSA. This was in line with the results shown in **Fig. 5A** where the same NP was shown to cause a decrease in the helicity of HSA. The unfolding behavior characterized by the peak at 208 nm **(Fig. 6B)** was strikingly different as compared to control HSA solutions. This could be attributed to NP-induced modifications on the HSA secondary structure, particularly on the ππ*

parallel transitions. The disappearance of the band at 208 nm at high temperatures (>70 °C) can be taken as evidence for the modifications of the melting behavior of HSA resulting from structural changes due to their contact with the NPs.

On the opposite, the thermal behavior of HSA has not been affected by the incubation with PLGA-PEG NPs, as the characteristic bands were fully maintained **(Fig. 6C)**. A more compact HSA structure was observed, suggesting that the protein has gained thermal stability. It is worth mentioning that HSA denaturation depends on its concentration and experimental conditions [21],[67]. Thus, in this study, given that all the experimental conditions were the same, qualitative comparisons could be made between HSA samples incubated or not with NPs. The key discovery was the alterations in HSA stability when it came into contact with PLGA NPs, despite the fact that they did not adsorb onto their surfaces. **(Fig. 2)**.

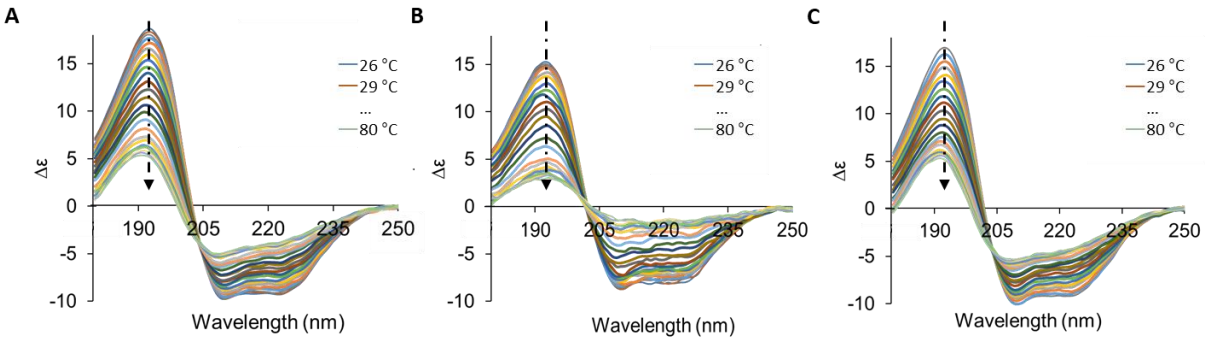

Fig. 7. Thermal unfolding of HSA followed by SRCD spectroscopy studied as a function of temperature over a range from 26 to 80 °C with intervals of 3 °C. **A**) control HSA (1mg/mL), **B**) HSA: nanoMOF (HSA: NP ratio of 1:3), **C**) HSA: nanoMOF-PEG (HSA: NP ratio of 1:3). All samples were analyzed after 2h of incubation.

Thermal denaturation profiles of HSA incubated with nanoMOF and nanoMOF-PEG were depicted in **Fig. 7**. Results were similar to the ones of PLGA and PLGA-PEG NPs. HSA was in a more unfolded state after incubation with the nanoMOF, and in particular, its characteristic band at 208 nm was diminished when increasing the temperature **(Fig. 7B)**. Moreover, HSA unfolding occurred, as the isosbestic point was sifted from 204 nm (HSA reference) to 202 nm (HSA in contact with the nanoMOFs). However, in the case of nanoMOF-PEG, there were no significant modifications neither on the characteristic band

at 208 nm nor on the isosbestic point **(Fig. 7C)**. The protein was maintained in a more folded state upon heating and remarkably preserved its compact form throughout the temperature increase. It can be therefore concluded that the PEG-based coating conferred thermal stabilization to the HSA molecules. This is also clearly shown in **Fig. 8,** presenting the melting curves of reference HSA, and HSA after contact with each NP. The protective effect of the PEG coatings on both PLGA and nanoMOFs is in line with the previous CZE findings [68][69].

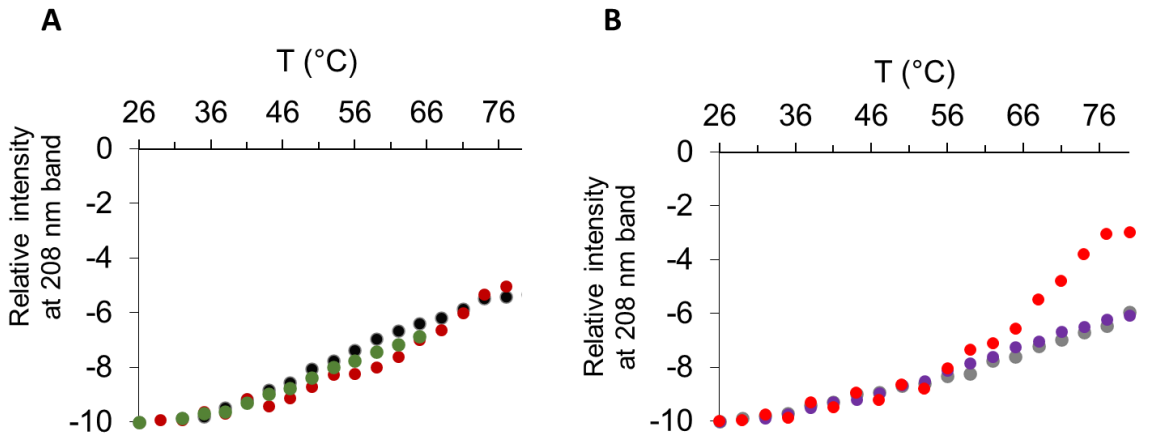

Fig. 8. Melting curves of HSA: **A)** Reference HSA (black) (incubated without NPs for 3 days), HSA incubated with during 3 days with PLGA (brown) and PLGA-PEG (green), HSA: NP ratio of 1:10 **B)** Reference HSA (grey) ((incubated without NPs for 2 hours), nanoMOF (purple) and nanoMOF-PEG (red) incubated with HSA during 2h, HSA: NP ratio of 1:3.

Conclusion

A set of orthogonal techniques was used here to investigate the interactions between HSA, the most abundant protein in the blood, and a series of NPs of similar mean diameters, surface-modified with PEG shells or left unmodified. Quantitative insights were gained using LC-MS and a protein assay kit. We discovered that although HSA didn't adsorb onto PLGA NPs, it underwent dramatic structural changes upon contact with these NPs. Indeed, the Cys form of HSA was particularly affected, and our studies revealed the appearance of new forms yet to be identified. In contrast to PLGA NPs, nanoMOFs adsorbed rapidly high

amounts of HSA, but the protein forms were unaffected by these interactions. Secondary structures of HSA and melting curves were also investigated by SR-CD. In all cases, the PEG protective layers avoided protein unfolding. However, the finding concerning HSA structural changes after interaction with PLGA NPs is of paramount importance as a conformational modification could alter HSA physiological properties (eg. Carriers for hormones, peptides, drugs…) and could lead to the formation of small aggregates. This feature could also have an impact on some other blood proteins.

As biocompatible NPs are gaining increasing interest for biomedical applications, a thorough understanding of their effects on the structure and functions of proteins is essential. The methodology proposed here could be applied to other types of NPs, loaded or not with drugs, as well as to other proteins known to interact with NPs in the bloodstream, such as immunoglobulins, complement, fibronectin etc. Moreover, in line with ethical issues, *in vitro* orthogonal methodologies to study NP-protein interactions are essential prior to *in vivo* experiments. In a broader view, the methodology developed in this work may be applied to evaluate the impact and safety of a variety of NPs engineered for intravenous administration.

Acknowledgements

We thank Stéphanie Yen-Nicolaÿ from the Plateforme de Protéomique (Ingénierie et Plateformes au Service de l'Innovation Thérapeutique, Chatenay Malabry, France) for help with LC-MS investigations and fruitful discussions. SR-CD measurements on DISCO beamline at SOLEIL Synchrotron light source were performed under the proposals 20180883 and 20171494. We thank Matthieu REFREGIERS and Frank WIEN for welcoming us to the DISCO beamline. This work is supported by a public grant overseen by the French National Research Agency (ANR) as part of the "Investissements d'Avenir" program (Labex NanoSaclay, reference: ANR-10-LABX-0035), and by ANR-20-CE19-0020.

Author contribution

Conceived the study: RG, CS. Performed the experiments: MSU, JMJ, XL, MAT. Data treatment: MSU, JMJ, FW, CS, RG. Wrote the manuscript: MSU, RG. Funding acquisition: RG, CS. All authors have read and agreed to the published version of the manuscript.

References

1. Mitchell MJ, Billingsley MM, Haley RM, Wechsler ME, Peppas NA, Langer R (2021) Engineering precision nanoparticles for drug delivery. Nat Rev Drug Discov 20:101–124. https://doi.org/10.1038/s41573-020-0090-8

2. Ventola CL (2017) Progress in nanomedicine: Approved and investigational nanodrugs. P and T 42:742–755

3. Kim HR, Andrieux K, Delomenie C, Chacun H, Appel M, Desmaële D, Taran F, Georgin D, Couvreur P, Taverna M (2007) Analysis of plasma protein adsorption onto PEGylated nanoparticles by complementary methods: 2-DE, CE and Protein Lab-on-chip® system. Electrophoresis 28:2252–2261. https://doi.org/10.1002/elps.200600694

4. Nakanishi K, Sakiyama T, Imamura K (2001) On the adsorption of proteins on solid surfaces, a common but very complicated phenomenon. J Biosci Bioeng 91:233–244. https://doi.org/10.1016/S1389-1723(01)80127-4

5. Lundqvist M, Stigler J, Elia G, Lynch I, Cedervall T, Dawson KA (2008) Nanoparticle size and surface properties determine the protein corona with possible implications for biological impacts. Proceedings of the National Academy of Sciences 105:14265–14270. https://doi.org/10.1073/pnas.0805135105

6. Nel AE, Mädler L, Velegol D, Xia T, Hoek EM V., Somasundaran P, Klaessig F, Castranova V, Thompson M (2009) Understanding biophysicochemical interactions at the nano–bio interface. Nat Mater 8:543–557. https://doi.org/10.1038/nmat2442

7. Schöttler S, Landfester K, Mailänder V (2016) Controlling the Stealth Effect of Nanocarriers through Understanding the Protein Corona. Angewandte Chemie International Edition 55:8806–8815. https://doi.org/10.1002/anie.201602233

8. Yesylevskyy SO, Ramseyer C, Savenko M, Mura S, Couvreur P (2018) Low-Density Lipoproteins and Human Serum Albumin as Carriers of Squalenoylated Drugs: Insights from Molecular Simulations. Mol Pharm 15:585–591. https://doi.org/10.1021/acs.molpharmaceut.7b00952

9. Gobeaux F, Bizeau J, Samson F, Marichal L, Grillo I, Wien F, Yesylevsky SO, Ramseyer C, Rouquette M, Lepêtre-Mouelhi S, Desmaële D, Couvreur P, Guenoun P, Renault JP, Testard F (2020) Albumin-driven disassembly of lipidic nanoparticles: The specific case of the squalene-adenosine nanodrug. Nanoscale 12:2793–2809. https://doi.org/10.1039/c9nr06485k

10. Tenzer S, Docter D, Kuharev J, Musyanovych A, Fetz V, Hecht R, Schlenk F, Fischer D, Kiouptsi K, Reinhardt C, Landfester K, Schild H, Maskos M, Knauer SK, Stauber RH (2013) Rapid formation of plasma protein corona critically affects nanoparticle pathophysiology. Nat Nanotechnol 8:772–781. https://doi.org/10.1038/nnano.2013.181

11. Rampado R, Crotti S, Caliceti P, Pucciarelli S, Agostini M (2020) Recent Advances in Understanding the Protein Corona of Nanoparticles and in the Formulation of “Stealthy” Nanomaterials. Front Bioeng Biotechnol 8:. https://doi.org/10.3389/fbioe.2020.00166

12. Papini E, Tavano R, Mancin F (2020) Opsonins and Dysopsonins of Nanoparticles: Facts, Concepts, and Methodological Guidelines. Front Immunol 11:. https://doi.org/10.3389/fimmu.2020.567365

13. Mariam J, Sivakami S, Dongre PM (2016) Albumin corona on nanoparticles–a strategic approach in drug delivery. Drug Deliv 23:2668–2676. https://doi.org/10.3109/10717544.2015.1048488

14. Lu X, Xu P, Ding HM, Yu YS, Huo D, Ma YQ (2019) Tailoring the component of protein corona via simple chemistry. Nat Commun 10:. https://doi.org/10.1038/s41467-019-12470-5

15. Lundqvist M, Sethson I, Jonsson BH (2004) Protein adsorption onto silica nanoparticles: Conformational changes depend on the particles’ curvature and the protein stability. Langmuir 20:10639–10647. https://doi.org/10.1021/la0484725

16. Satzer P, Svec F, Sekot G, Jungbauer A (2016) Protein adsorption onto nanoparticles induces conformational changes: Particle size dependency, kinetics, and mechanisms. Eng Life Sci 16:238–246. https://doi.org/10.1002/elsc.201500059

17. Saptarshi SR, Duschl A, Lopata AL (2013) Interaction of nanoparticles with proteins: relation to bio-reactivity of the nanoparticle. J Nanobiotechnology 11:26. https://doi.org/10.1186/1477-3155-11-26

18. Shemetov AA, Nabiev I, Sukhanova A (2012) Molecular Interaction of Proteins and Peptides with Nanoparticles. ACS Nano 6:4585–4602. https://doi.org/10.1021/nn300415x

19. Verrecchia T, Huve P, Bazile D, Veillard M, Spenlehauer G, Couvreur P (1993) Adsorption/desorption of human serum albumin at the surface of poly(lactic acid) nanoparticles prepared by a solvent evaporation process. J Biomed Mater Res 27:1019–1028. https://doi.org/10.1002/jbm.820270807

20. Lindman S, Lynch I, Thulin E, Nilsson H, Dawson KA, Linse S (2007) Systematic investigation of the thermodynamics of HSA adsorption to N-iso-propylacrylamide/N-tert-butylacrylamide copolymer nanoparticles. Effects of particle size and hydrophobicity. Nano Lett 7:914–920. https://doi.org/10.1021/nl062743+

21. Laera S, Ceccone G, Rossi F, Gilliland D, Hussain R, Siligardi G, Calzolai L (2011) Measuring protein structure and stability of protein-nanoparticle systems with synchrotron radiation circular dichroism. Nano Lett 11:4480–4484. https://doi.org/10.1021/nl202909s

22. Teichroeb JH, Forrest JA, Jones LW (2008) Size-dependent denaturing kinetics of bovine serum albumin adsorbed onto gold nanospheres. European Physical Journal E 26:411–415. https://doi.org/10.1140/epje/i2007-10342-9

23. Yang X, Bolsa-Ferruz M, Marichal L, Porcel E, Salado-Leza D, Lux F, Tillement O, Renault J-P, Pin S, Wien F, Lacombe S (2020) Human Serum Albumin in the Presence of AGuIX Nanoagents: Structure Stabilisation without Direct Interaction. Int J Mol Sci 21:4673. https://doi.org/10.3390/ijms21134673

24. Devineau S, Kiger L, Galacteros F, Baudin-Creuza V, Marden M, Renault JP, Pin S (2018) Manipulating hemoglobin oxygenation using silica nanoparticles: a novel prospect for artificial oxygen carriers. Blood Adv 2:90–94. https://doi.org/10.1182/bloodadvances.2017012153

25. Peracchia MT, Harnisch S, Pinto-Alphandary H, Gulik A, Dedieu JC, Desmaële D, d'Angelo J, Müller RH, Couvreur P (1999) Visualization of in vitro protein-rejecting properties of PEGylated stealth® polycyanoacrylate nanoparticles. Biomaterials 20:1269–1275. https://doi.org/10.1016/S0142-9612(99)00021-6

26. Cutrone, Li, Casas-Solvas, Menendez-Miranda, Qiu, Benkovics, Constantin, Malanga, Moreira-Alvarez, Costa-Fernandez, García-Fuentes, Gref, Vargas-Berenguel (2019) Design of Engineered Cyclodextrin Derivatives for Spontaneous Coating of Highly Porous Metal-Organic Framework Nanoparticles in Aqueous Media. Nanomaterials 9:1103. https://doi.org/10.3390/nano9081103

27. Agostoni V, Horcajada P, Noiray M, Malanga M, Aykaç A, Jicsinszky L, Vargas-Berenguel A, Semiramoth N, Daoud-Mahammed S, Nicolas V, Martineau C, Taulelle F, Vigneron J, Etcheberry A, Serre C, Gref R (2015) A "green" strategy to construct non-covalent, stable and bioactive coatings on porous MOF nanoparticles. Sci Rep 5:7925. https://doi.org/10.1038/srep07925

28. Cedervall T, Lynch I, Lindman S, Berggård T, Thulin E, Nilsson H, Dawson KA, Linse S (2007) Understanding the nanoparticle-protein corona using methods to quntify exchange rates and affinities of proteins for nanoparticles. Proc Natl Acad Sci U S A 104:2050–2055. https://doi.org/10.1073/pnas.0608582104

29. Fornaguera C, Calderó G, Mitjans M, Vinardell MP, Solans C, Vauthier C (2015) Interactions of PLGA nanoparticles with blood components: Protein adsorption, coagulation, activation of the complement system and hemolysis studies. Nanoscale 7:6045–6058. https://doi.org/10.1039/c5nr00733j

30. Linse S, Cabaleiro-Lago C, Xue WF, Lynch I, Lindman S, Thulin E, Radford SE, Dawson KA (2007) Nucleation of protein fibrillation by nanoparticles. Proc Natl Acad Sci U S A 104:8691–8696. https://doi.org/10.1073/pnas.0701250104

31. Davidson AM, Brust M, Cooper DL, Volk M (2017) Sensitive Analysis of Protein Adsorption to Colloidal Gold by Differential Centrifugal Sedimentation. Anal Chem 89:6807–6814. https://doi.org/10.1021/acs.analchem.7b01229

32. Duan Y, Liu Y, Shen W, Zhong W (2017) Fluorescamine Labeling for Assessment of Protein Conformational Change and Binding Affinity in Protein-Nanoparticle Interaction. Anal Chem 89:12160–12167. https://doi.org/10.1021/acs.analchem.7b02810

33. De Paoli Lacerda SH, Park JJ, Meuse C, Pristinski D, Becker ML, Karim A, Douglas JF (2010) Interaction of gold nanoparticles with common human blood proteins. ACS Nano 4:365–379. https://doi.org/10.1021/nn9011187

34. Kharazian B, Hadipour NL, Ejtehadi MR (2016) Understanding the nanoparticle-protein corona complexes using computational and experimental methods. International Journal of Biochemistry and Cell Biology 75:162–174

35. Saptarshi SR, Duschl A, Lopata AL (2013) Interaction of nanoparticles with proteins: Relation to bio-reactivity of the nanoparticle. J Nanobiotechnology 11:1. https://doi.org/10.1186/1477-3155-11-26

36. Lee H (2020) Effects of Nanoparticle Electrostatics and Protein–Protein Interactions on Corona Formation: Conformation and Hydrodynamics. Small 16:1906598. https://doi.org/10.1002/smll.201906598

37. Böhmert L, Voß L, Stock V, Braeuning A, Lampen A, Sieg H (2020) Isolation methods for particle protein corona complexes from protein-rich matrices. Nanoscale Adv 2:563–582. https://doi.org/10.1039/c9na00537d

38. Ural MS, Menéndez-Miranda M, Salzano G, Mathurin J, Aybeke EN, Deniset-Besseau A, Dazzi A, Porcino M, Martineau-Corcos C, Gref R (2021) Compartmentalized Polymeric Nanoparticles Deliver Vancomycin in a pH-Responsive Manner. Pharmaceutics 13:1992. https://doi.org/10.3390/pharmaceutics13121992

39. Agostoni V, Chalati T, Horcajada P, Willaime H, Anand R, Semiramoth N, Baati T, Hall S, Maurin G, Chacun H, Bouchemal K, Martineau C, Taulelle F, Couvreur P, Rogez-Kreuz C, Clayette P, Monti S, Serre C, Gref R (2013) Towards an Improved anti-HIV Activity of NRTI via Metal–Organic Frameworks Nanoparticles. Adv Healthc Mater 2:1630–1637. https://doi.org/10.1002/adhm.201200454

40. Qiu J, Li X, Steenkeste K, Barroca-Aubry N, Aymes-Chodur C, Roger P, Casas-Solvas JM, Vargas-Berenguel A, Rihouey C, Picton L, Gref R (2020) Self-assembled multifunctional core–shell highly porous metal–organic framework nanoparticles. Int J Pharm 581:119281. https://doi.org/10.1016/j.ijpharm.2020.119281

41. Rossi E, Tran NT, Hirtz C, Lehmann S, Taverna M (2020) Efficient extraction of intact HSA-Aβ peptide complexes from sera: Toward albuminome biomarker identification. Talanta 216:121002. https://doi.org/10.1016/j.talanta.2020.121002

42. Lees JG, Smith BR, Wien F, Miles AJ, Wallace BA (2004) CDtool - An integrated software package for circular dichroism spectroscopic data processing, analysis, and archiving. Anal Biochem 332:285–289. https://doi.org/10.1016/j.ab.2004.06.002

43. Micsonai A, Wien F, Kernya L, Lee YH, Goto Y, Réfrégiers M, Kardos J (2015) Accurate secondary structure prediction and fold recognition for circular dichroism spectroscopy. Proc Natl Acad Sci U S A 112:E3095–E3103. https://doi.org/10.1073/pnas.1500851112

44. Wien F, Wallace BA (2005) Calcium fluoride micro cells for synchrotron radiation circular dichroism spectroscopy. Appl Spectrosc 59:1109–1113. https://doi.org/10.1366/0003702055012546

45. Miles AJ, Janes RW, Brown A, Clarke DT, Sutherland JC, Tao Y, Wallace BA, Hoffmann S V. (2008) Light flux density threshold at which protein denaturation is induced by synchrotron radiation circular dichroism beamlines. J Synchrotron Radiat 15:420–422. https://doi.org/10.1107/S0909049508009606

46. Wien F, Miles AJ, Lees JG, Vrønning Hoffmann S, Wallace BA (2005) VUV irradiation effects on proteins in high-flux synchrotron radiation circular dichroism spectroscopy. J Synchrotron Radiat 12:517–523. https://doi.org/10.1107/S0909049505006953

47. Gref R, Minamitake Y, Peracchia MT, Trubetskoy V, Torchilin V, Langer R (1994) Biodegradable long-circulating polymeric nanospheres. Science (1979) 263:1600–1603. https://doi.org/10.1126/science.8128245

48. Zambaux MF, Bonneaux F, Gref R, Maincent P, Dellacherie E, Alonso MJ, Labrude P, Vigneron C (1998) Influence of experimental parameters on the characteristics of poly(lactic acid) nanoparticles prepared by a double emulsion method. Journal of Controlled Release 50:31–40. https://doi.org/10.1016/S0168-3659(97)00106-5

49. Tobío M, Gref R, Sánchez A, Langer R, Alonso MJ (1998) Stealth PLA-PEG nanoparticles as protein carriers for nasal administration. Pharm Res 15:270–275. https://doi.org/10.1023/A:1011922819926

50. Horcajada P, Chalati T, Serre C, Gillet B, Sebrie C, Baati T, Eubank JF, Heurtaux D, Clayette P, Kreuz C, Chang JS, Hwang YK, Marsaud V, Bories PN, Cynober L, Gil S, Férey G, Couvreur P, Gref R (2010) Porous metal-organic-framework nanoscale carriers as a potential platform for drug deliveryand imaging. Nat Mater 9:172–178. https://doi.org/10.1038/nmat2608

51. Baati T, Njim L, Neffati F, Kerkeni A, Bouttemi M, Gref R, Najjar MF, Zakhama A, Couvreur P, Serre C, Horcajada P (2013) In depth analysis of the in vivo toxicity of nanoparticles of porous iron(iii) metal–organic frameworks. Chem Sci 4:1597–1607. https://doi.org/10.1039/c3sc22116d

52. Li X, Salzano G, Qiu J, Menard M, Berg K, Theodossiou T, Ladavière C, Gref R (2020) Drug-Loaded Lipid-Coated Hybrid Organic-Inorganic “Stealth” Nanoparticles for Cancer Therapy. Front Bioeng Biotechnol 8:1027. https://doi.org/10.3389/fbioe.2020.01027

53. Li X, Lachmanski L, Safi S, Sene S, Serre C, Grenèche JM, Zhang J, Gref & R New insights into the degradation mechanism of metal-organic frameworks drug carriers OPEN. https://doi.org/10.1038/s41598-017-13323-1

54. Christodoulou I, Serre C, Gref R (2020) Metal-organic frameworks for drug delivery: Degradation mechanism and in vivo fate. In: Metal-Organic Frameworks for Biomedical Applications. Elsevier, pp 467–489

55. Ramírez-García G, d'Orlyé F, Gutiérrez-Granados S, Martínez-Alfaro M, Mignet N, Richard C, Varenne A (2017) Electrokinetic Hummel-Dreyer characterization of nanoparticle-plasma protein corona: The non-specific interactions between PEG-modified persistent luminescence nanoparticles and albumin. Colloids Surf B Biointerfaces 159:437–444. https://doi.org/10.1016/j.colsurfb.2017.08.012

56. Marie A-L, Tran NT, Taverna M (2016) Characterization of Chemical and Physical Modifications of Human Serum Albumin by Capillary Zone Electrophoresis. pp 151–163

57. Marie A-L, Przybylski C, Gonnet F, Daniel R, Urbain R, Chevreux G, Jorieux S, Taverna M (2013) Capillary zone electrophoresis and capillary electrophoresis-mass spectrometry for analyzing qualitative and quantitative variations in therapeutic albumin. Anal Chim Acta 800:103–110. https://doi.org/10.1016/j.aca.2013.09.023

58. Coty JB, Varenne F, Benmalek A, Garsaa O, Le Potier I, Taverna M, Smadja C, Vauthier C (2018) Characterization of nanomedicines' surface coverage using molecular probes and capillary electrophoresis. European Journal of Pharmaceutics and Biopharmaceutics 130:48–58. https://doi.org/10.1016/j.ejpb.2018.06.014

59. Belder D, Deege A, Husmann H, Kohler F, Ludwig M (2001) Cross-linked poly(vinyl alcohol) as permanent hydrophilic column coating for capillary electrophoresis. Electrophoresis 22:3813–3818. https://doi.org/10.1002/1522-2683(200109)22:17<3813::AID-ELPS3813>3.0.CO;2-D

60. Bar-Or D, Bar-Or R, Rael LT, Gardner DK, Slone DS, Craun ML (2005) Heterogeneity and oxidation status of commercial human albumin preparations in clinical use*. Crit Care Med 33:1638–1641. https://doi.org/10.1097/01.CCM.0000169876.14858.91

61. Mao P, Wang D (2014) Top-Down Proteomics of a Drop of Blood for Diabetes Monitoring. J Proteome Res 13:1560–1569. https://doi.org/10.1021/pr401074t

62. Rogers DM, Jasim SB, Dyer NT, Auvray F, Réfrégiers M, Hirst JD (2019) Electronic Circular Dichroism Spectroscopy of Proteins. Chem 5:2751–2774. https://doi.org/10.1016/j.chempr.2019.07.008

63. Bulheller BM, Miles AJ, Wallace BA, Hirst JD (2008) Charge-transfer transitions in the vacuum-ultraviolet of protein circular dichroism spectra. Journal of Physical Chemistry B 112:1866–1874. https://doi.org/10.1021/jp077462k

64. Kamal JKA, Zhao L, Zewail AH (2004) Ultrafast hydration dynamics in protein unfolding: Human serum albumin. Proc Natl Acad Sci U S A 101:13411–13416. https://doi.org/10.1073/pnas.0405724101

65. Maciążek-Jurczyk M, Janas K, Pożycka J, Szkudlarek A, Rogóż W, Owczarzy A, Kulig K (2020) Human serum albumin aggregation/fibrillation and its abilities to drugs binding. Molecules 25:. https://doi.org/10.3390/molecules25030618

66. Bhattacharya M, Jain N, Mukhopadhyay S (2011) Insights into the Mechanism of Aggregation and Fibril Formation from Bovine Serum Albumin. J Phys Chem B 115:4195–4205. https://doi.org/10.1021/jp111528c

67. WETZEL R, BECKER M, BEHLKE J, BILLWITZ H, BoHM S, EBERT B, HAMANN H, KRUMBIEGEL J, LASSMANN G (1980) Temperature Behaviour of Human Serum Albumin. Eur J Biochem 104:469–478. https://doi.org/10.1111/j.1432-1033.1980.tb04449.x

68. Samanta N, Mahanta D Das, Hazra S, Kumar GS, Mitra RK (2014) Short chain polyethylene glycols unusually assist thermal unfolding of human serum albumin. Biochimie 104:81–89. https://doi.org/10.1016/j.biochi.2014.05.009

69. Das NK, Ghosh N, Kale AP, Mondal R, Anand U, Ghosh S, Tiwari VK, Kapur M, Mukherjee S (2014) Temperature Induced Morphological Transitions from Native to Unfolded Aggregated States of Human Serum Albumin. J Phys Chem B 118:7267–7276. https://doi.org/10.1021/jp5030944